Solar Energy Materials & Solar Cells 282 (2025) 113444

Contents lists available at ScienceDirect

Solar Energy Materials and Solar Cells

journal homepage: www.elsevier.com/locate/solmat

Alleviating contaminant-induced degradation of TOPCon solar cells with copper plating

Xutao Wang, Chandany Sen *, Xinyuan Wu, Yuan-Chih Chang, Haoran Wang, Muhammad Umair Khan, Bram Hoex **

School of Photovoltaic and Renewable Energy Engineering, University of New South Wales, Sydney, 2052, Australia

ARTICLE INFO

Keywords:
Reliability
TOPCon
Damp-heat degradation
Copper plating
Contaminant-induced degradation

ABSTRACT

With the development of silicon (Si) solar cell technology, the tunnel oxide passivated contact (TOPCon) architecture has become the dominant industrial technology in the solar market. At the same time, concerns are raised about the long-term stability of TOPCon photovoltaic modules. The front side metallization of TOPCon solar cells is reported to be susceptible to corrosion as identified during cell and module level damp-heat (DH) testing. In this work, we use copper (Cu) plating on screen-printed (Ag paste with up to 3 % Al) TOPCon solar cells to address this problem. The plated cells show an improved performance due to the higher fill factor, indicating the potential of reducing the silver (Ag) consumption and material cost without sacrificing the solar cell efficiency. NaCl was chosen as a representative contaminant to assess the reliability at the cell level after 6 h of DH. The Cu-plated TOPCon solar cells showed only a ~11.5%$_{rel}$ drop in efficiency, compared to ~80%$_{rel}$ reduction in efficiency for the as-received cells. We also show that the Cu plating process results in a considerably denser contact, which hinders the penetration of contaminants. Consequently, the method presented in this work enhances the stability of photovoltaic technology with corrosion-sensitive contacts during field operation, thus contributing to an increase in lifetime and reduction in levelized cost of electricity.

1. Introduction

According to the International Technology Roadmap for Photovoltaic (ITRPV) 2024 [1], n-type Si solar cells are predicted to dominate the mono-Si solar cell market from 2024. Tunnel oxide passivated contact (TOPCon) [2–5] and Si heterojunction (SHJ) [6–9] are expected to be the dominant solar cell architectures. In particular, TOPCon solar cells will account for over 50 % of the solar cell market share within the next 10 years [1]. Meanwhile, efficiencies up to 26.58 % have been achieved by large-area TOPCon solar cells [10,11].

For the levelized cost of electricity (LCOE) [12], both the initial efficiency and stability are of critical importance [13]. Still, manufacturers mainly focus on increasing the initial efficiency of solar cells with less focus on long-term stability. However, for economic and sustainability evaluation, longer warranties and better stability are critical [14]. As mono-Si single-junction solar cell efficiency keeps increasing and is approaching the theoretical limit [15], the relative impact of certain failure modes becomes higher. The damp-heat (DH) test [16] is a common accelerated stability test applied on photovoltaic modules to assess their sensitivity to humidity and temperature under long-term outdoor operation conditions. Numerous reliability issues, including a reduction in fill factor, increase in series resistance, decrease in open-circuit voltage, etc., after damp-heat testing have been reported [17–21]. Table 1 shows the previous work on the DH-related degradation of TOPCon cells and modules. In summary, the results show that severe degradation can be seen after DH testing, and the main sensitivity is related to the front metallization of TOPCon devices. All these findings indicate that this issue is not limited to certain manufacturers of TOPCon cells/modules and is an indication of a more generic sensitivity.

Normally, damp-heat degradation is caused by the combination of moisture, heat as well as contaminants that were either already present or formed in the module or entered during operation. Regarding the potential harmful contaminants, one particular contaminant of interest is sodium (Na). Na is commonly believed to be released from the soda-lime glass of modules [29–31]. The introduced Na could then induce degradation of power output, fill factor and open-circuit voltage

* Corresponding author.
** Corresponding author.
E-mail addresses: chandany.sen@unsw.edu.au (C. Sen), b.hoex@unsw.edu.au (B. Hoex).

https://doi.org/10.1016/j.solmat.2025.113444
Received 10 December 2024; Received in revised form 12 January 2025; Accepted 17 January 2025

Table 1
Summary of the previous study on the DH-related degradation of TOPCon cells/modules.

Previous work	Device	Test condition	Brief conclusion
N. Iqbal et al. [22]	Cell	~5 vol% acetic acid solution, up to 120 min	V_{oc} drop, contact resistance increase, front Ag finger degradation
P. M. Sommeling et al. [23]	Module	DH (85 °C/85 % RH), up to 2500 h	*FF* drop, front side metallization degradation induced by acid or moisture
Y. Zhou et al. [24]	Module	DH (85 °C/85 % RH), up to 3000 h	I_{sc} & *FF* drop, R_s increase, front side corrosion
C. Sen et al. [25]	Cell	DH (85 °C/85 % RH), 0.9 wt% NaCl solution, up to 20 h	V_{oc}, I_{sc} and *FF* drop, front metal delamination with the presence of Na^+ and Cl^- at the contact
X. Wu et al. [26]	Cell	DH (85 °C/85 % RH), 0.9 wt% NaCl solution, up to 40 h	V_{oc} drop, contact resistance increase, corrosion of front metal contact
	Module	DH (85 °C/85 % RH), up to 1000 h	I_{sc} & *FF* drop, failure along the contact
C. Sen et al. [27]	Module	DH (85 °C/85 % RH), up to 1000 h	V_{oc} & *FF* drop, failure related to moisture and contaminants
X. Wu et al. [28]	Cell	DH (85 °C/85 % RH), 0.155 mol/L NaCl or $NaHCO_3$ solution, up to 100 h	NaCl led to severe R_s increase and front side corrosion, while $NaHCO_3$ mainly led to V_{oc} drop at the rear.

[32–35]. Furthermore, Na can also be introduced into solar modules during operation with exposure to seawater, dust, rainwater, and soil, which can bring in a significant amount of chloride (Cl) as well [25,36–38]. The presence of Na and Cl is reported in the solar cells of failed modules (with increased series resistance, shunting, lower open-circuit voltage, etc.) after an extended period of operation in the field [39,40], illustrating that Na and Cl were able to penetrate the module and lead to performance degradation of solar devices. Additionally, NaCl has already been used to test salt mist corrosion on PV devices, as mentioned in IEC 61701 [41]. Therefore, it is reasonable to use NaCl as a potential contaminant to assess the damp-heat reliability of solar devices. Recently, our research group [25] reported severe degradation of TOPCon and SHJ solar cells compared to passivated emitter and rear cells (PERC) when the solar cells were exposed to NaCl before damp-heat testing. Among them, TOPCon was found to degrade the most, particularly on the highly sensitive front side. This finding is consistent with previous studies involving other contaminants.

Fortunately, there have been some reports of mitigation solutions for these kinds of corrosion-related failures. It was shown that barrier layers (SiO_x [32,42], AlO_x [33]) are effective in protecting SHJ cells from contaminant (including Na^+) related degradation. Our group recently reported [26] that the use of paste with a low or no Al content on the front enabled by laser-enhanced contact firing significantly enhanced the damp-heat stability of TOPCon solar cells and modules. In this work, we report on another method to improve the stability of TOPCon solar cells by adding a plating process without any changes to the traditional paste or firing process. The in-diffusion of harmful contaminants is regarded as a highly possible cause for the degradation of TOPCon solar cells under DH conditions [25]. Therefore, preventing contaminants from infiltrating the metal contacts may be an appealing way to protect the solar cells from degradation. One way to achieve this objective is metal plating, which has previously been shown to fill the voids of contacts and make them more compact [43] thereby potentially making the contacts less sensitive to degradation. Thus, in this work, we plated Cu on the front side to assess its protective effect under DH conditions. The DH reliability test was conducted at the cell level which is up to two orders of magnitude quicker than at the module level [25]. Notably, the plated-Cu contact should typically be capped with Ag or Sn [44–48] to prevent oxidation and improve the soldering process. However, this study mainly focused on the protective effect of plated-Cu on contaminant-induced degradation, so no more capping layers were added. According to the characterization results, the plated-Cu was found to show a superior protective effect and highly alleviated the NaCl-induced degradation after 6 h of DH testing. Besides, the self-alignment plating process has the potential to reduce silver consumption and costs without compromising electrical performance. These combined effects could significantly contribute to lowering the levelized cost of energy (LCOE) and enhancing sustainability.

2. Methodology

Bifacial nine-busbar (9BB) 158 mm TOPCon solar cells were used in this work. The TOPCon cells featured a tunneling SiO_x/phosphorus-doped poly silicon (n^+ poly-Si)/SiN_x stack and a screen-printed H-pattern silver grid (Al-free Ag paste) on the rear. The front side featured a boron-doped emitter (p^+ emitter), AlO_x/SiN_x stack, and a screen-printed H-pattern silver grid (Al-containing Ag paste) as shown in Fig. 1 (a). As the cells were sourced prior to 2023, no laser-assisted firing was used in the fabrication process. The plating process was done on screen-printed solar cells by using a Conifer plating tool at the Solar Industrial Research Facility (SIRF) at UNSW. As reported [25], NaCl seriously affects the performance of TOPCon cells during DH testing when applied on the front of cells, while the rear side of TOPCon was found to be stable. Therefore, we plated a ~1 μm (estimated from plating rate) Cu layer on the front side of TOPCon solar cells to test its protective effect. The design of the experiment is shown in Fig. 1 (b). Samples were cleaned with deionized water (DIW) before the plating. During the plating process, the rear side completely contacted the cathode electrode, and the front side was immersed in the plating solution ($CuSO_4$). A bias-assisted light-induced plating (LIP) was applied with a ~150 mA constant current and illumination during the process. Before the damp heat testing, all of the samples were cleaned with deionized water (DIW) followed by nitrogen (N_2) drying before the test to ensure they were clean. Then, a ~0.9 % weight (medical-grade) NaCl solution was sprayed uniformly on the front side of bare (Group Bare_NaCl) and plated (Group Plated_NaCl) cells. After that, all of the cells were put into an ASLi Environment chamber for an 85 °C and 85 % relative humidity accelerated damp-heat (DH) testing. Moreover, plated and non-plated cell stripes without busbars were cut by a FOBA M1000 scribing laser tool. Then we measured the contact resistivity of those samples at intervals during the DH testing.

The one-sun current-voltage (I-V) parameters of cells were measured by a LOANA I-V tester from pv-tools. A BTi (LIS-R3) luminescence imaging system was used to capture the photoluminescence (PL) and series resistance (R_s) images with a high open-circuit voltage lens. PL images were processed by LumiTools [49] and R_s images were analyzed by ImageJ [50]. A pv-tools TLM-SCAN$^+$ tool was used to carry out the transfer length method (TLM) measurement at intervals during the DH testing to extract the contact resistance. A four-point probe station was used to measure the line resistance of solar cells. Top-view scanning electron microscopy (SEM) images were taken by a FEI Nova NanoSEM 450 FE-SEM, while a ZEISS Cryogenic focused ion beam (Cryo-FIB)-SEM tool was used to cut through the finger contact of cells and take cross-sectional SEM images as well. The energy dispersive spectroscopy (EDS) data was measured by the Oxford Instruments Ultim® Max and analyzed with AZtec software.

3. Results and discussion

3.1. Performance of the as-plated cells

The top-view SEM images on the front metal of bare and as-plated samples are shown in Fig. 2. As shown in Fig. 2 (a), the metal contact of the bare sample showed a highly porous structure. As shown in Fig. 2

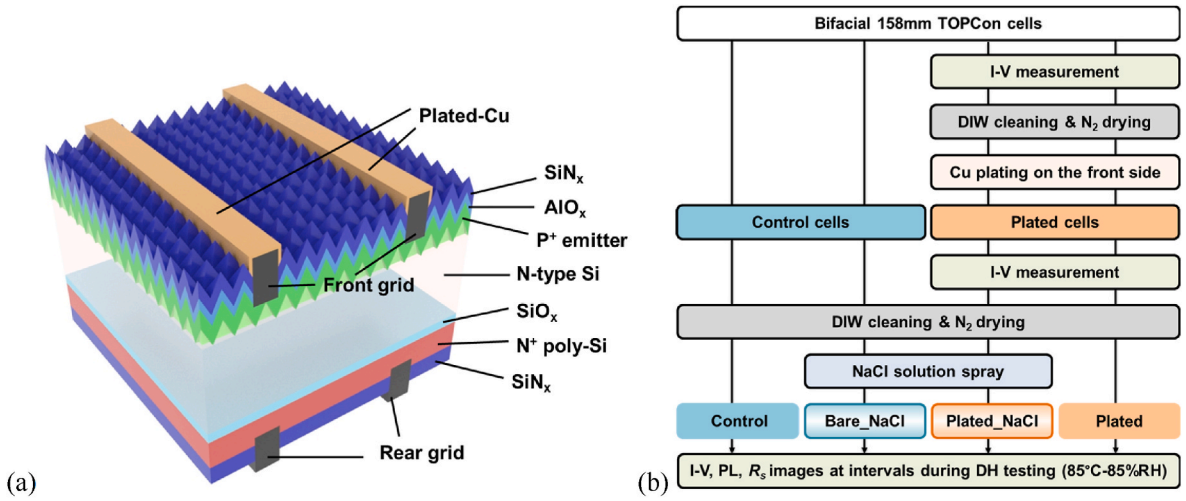

Fig. 1. (a) Schematic of TOPCon solar cells with Cu plated on the front grid, and (b) experimental flow chart used in this work.

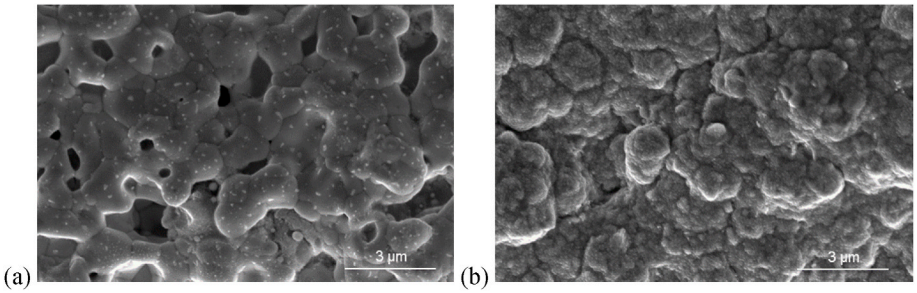

Fig. 2. Top-view SEM images of the front metal contact of the (a) as-received and (b) plated sample.

(b), the Cu-plated contact did not show any pores. In Fig. 3, the top-view EDS results demonstrate that the plated-Cu covers the screen-printed metal surface very well. The Ag signal could hardly be detected after the plating process, except for some scattered Ag particles outside of the finger regions.

A cryo-FIB was utilized to cut through the fingers and subsequently capture cross-sectional SEM and EDS results for detailed analysis. In Fig. 4, the images of the front metal of as-received and plated samples are shown. The capping layer of the samples is coated Pt for FIB sample preparation after the DH test, and it has no adverse effects on the subsequent analysis. In Fig. 4 (a), the finger bulk showed structures with high porosity, which was consistent with what we observed on the metal surface. Importantly, the Cu signal of the plated sample shown in Fig. 4 (b) illustrated that the Cu layer completely covered the surface of the contact and even filled some voids in the metal bulk, as long as those voids were accessible by the plating solution during the plating process.

However, Cu also has well-known problems for solar cell application, especially the diffusion into Si. It is reported that Cu can penetrate into Si, form deep-level traps and lead to parasitic recombination in solar cells [51–53]. Fortunately, the Cu layer, in our case, was separated from the Si bulk by the SiN_x/AlO_x passivation layer and the screen-printed metal contact. Both of them were reported to serve as an effective barrier layer to hinder Cu diffusion under normal operation conditions [54–56]. Therefore, we do not expect our cells to suffer from Cu in-diffusion. Additionally, the complete cell should also be capped with Ag or Sn to prevent Cu oxidation and assist the soldering process.

Table 2 summarizes the electrical performance of samples before and after the plating process. It is notable that the *PCE* of samples improved by ~0.09%$_{abs}$ after the plating process, with no significant changes observed in V_{oc}. The high-density plated-Cu layer reduced the line resistance of fingers and busbars, which was probably the main reason for the ~0.56%$_{abs}$ higher fill factor (*FF*) [57]. On the contrary, the additional Cu layer increases the size of the front metal contact, thereby increasing shading, leading to a ~0.12 mA/cm^2 lower J_{sc}, as shown in Table 2. The increased *FF* and decreased J_{sc} could also be confirmed by the current-voltage curve with locally magnified images, as shown in Fig. 5. Moreover, the overall improved efficiency caused by lower metal resistance also showed the potential of reducing Ag usage and material cost [57], by replacing part of the screen-printed Ag on the top with plated-Cu, which may reduce the LCOE of the technology.

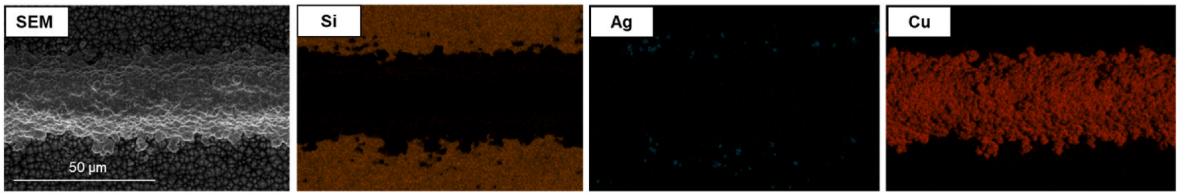

Fig. 3. Top-view EDS images of the front metal contact after the plating process, with EDS mapping of elements Si, Ag, and Cu.

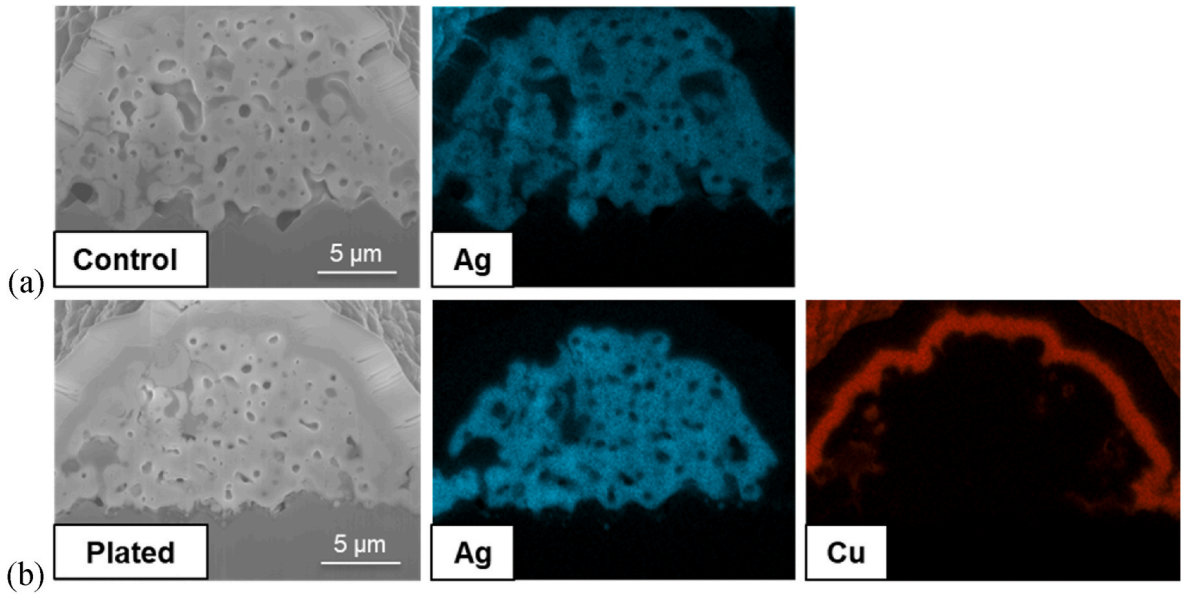

Fig. 4. Cross-sectional SEM images of (a) as-received and (b) plated samples and corresponding EDS mappings for Ag (both samples) and Cu (plated sample only).

Table 2
FF, V_{oc}, J_{sc}, and *PCE*, as well as the corresponding standard deviation of the as-received and plated solar cells. The absolute variations were calculated based on the mean value of each parameter before and after plating.

	PCE (%)	V_{oc} (mV)	J_{sc} (mA/cm^2)	*FF* (%)
Before Plating	23.24 ± *0.03*	706.4 ± *1.6*	39.79 ± *0.08*	82.68 ± *0.27*
After Plating	23.33 ± *0.06*	706.6 ± *1.7*	39.67 ± *0.10*	83.23 ± *0.12*
Absolute Variation	0.09	0.1	−0.12	0.56

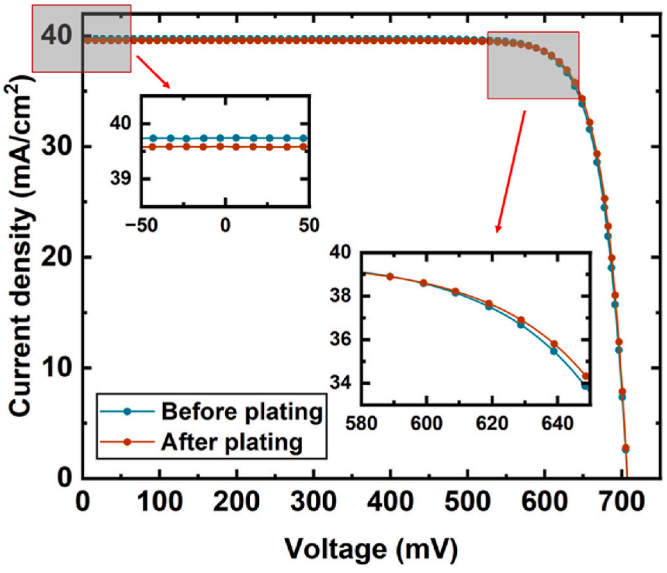

Fig. 5. Current-voltage curve of a representative cell before and after the plating process.

3.2. Accelerated damp-heat testing of TOPCon solar cells

After evaluating the performance of as-plated cells, their protective effects against NaCl-induced degradation were assessed by accelerated damp-heat testing, together with bare samples without plated-Cu, as shown in Fig. 1 (b).

3.2.1. I-V results during DH testing

Fig. 6 shows the I-V parameters of cells from different groups, as shown in Fig. 1 (b), as a function of the damp heat testing time. The Control samples remained stable, indicating that the high-temperature and high-humidity damp-heat test by itself did not induce degradation of TOPCon solar cells. Additionally, no significant degradation was observed in the plated samples after the DH testing. The results further confirmed that the plated-Cu was not detrimental to cells and also remained stable under conditions of 85 % relative humidity and 85 °C. However, losses can be observed in the bare cells exposed to NaCl (Bare_NaCl) during the DH testing. After 6 h of DH testing, a significant rise in R_s was observed, which was found to be nearly 50 times higher than the initial value. The relative ~52.2 % lower short-circuit current density (J_{sc}) indicated a reduced carrier collection ability after DH testing, and the ~2.8%$_{rel}$ drop of open-circuit voltage (V_{oc}) illustrated some induced recombination, potentially due to metal ion infiltration from the corroded contacts and the contaminants introduced for accelerated DH testing. Overall, the 6 h of DH testing led to over 80 % relative degradation of *PCE* for the Bare_NaCl sample. The severe degradation of TOPCon samples is in good agreement with our previous work [25,28].

Interestingly, in contrast to the Bare_NaCl samples, the Plated_NaCl samples only presented a relatively minor drop (~11.5%$_{rel}$) in *PCE* after 6 h of DH testing. There was just a ~1.2%$_{rel}$ J_{sc} drop for the Plated_NaCl samples after the DH testing and only a ~0.2%$_{rel}$ V_{oc} drop. The performance degradation was mainly caused by a ~10.2 % decrease in *FF*, which could be mostly attributed to an increase in R_s (around 5 times higher). However, the *FF* loss was still significantly lower compared to the Bare_NaCl samples (~64.6%$_{rel}$ loss after 6 h of DH testing). Overall, the Bare_NaCl sample just showed an end-of-life efficiency of less than 5 %, while the Plated_NaCl sample still maintained an efficiency of higher than 20 %. Consequently, Cu-plating was found to be highly effective in alleviating the NaCl-induced degradation during the DH testing.

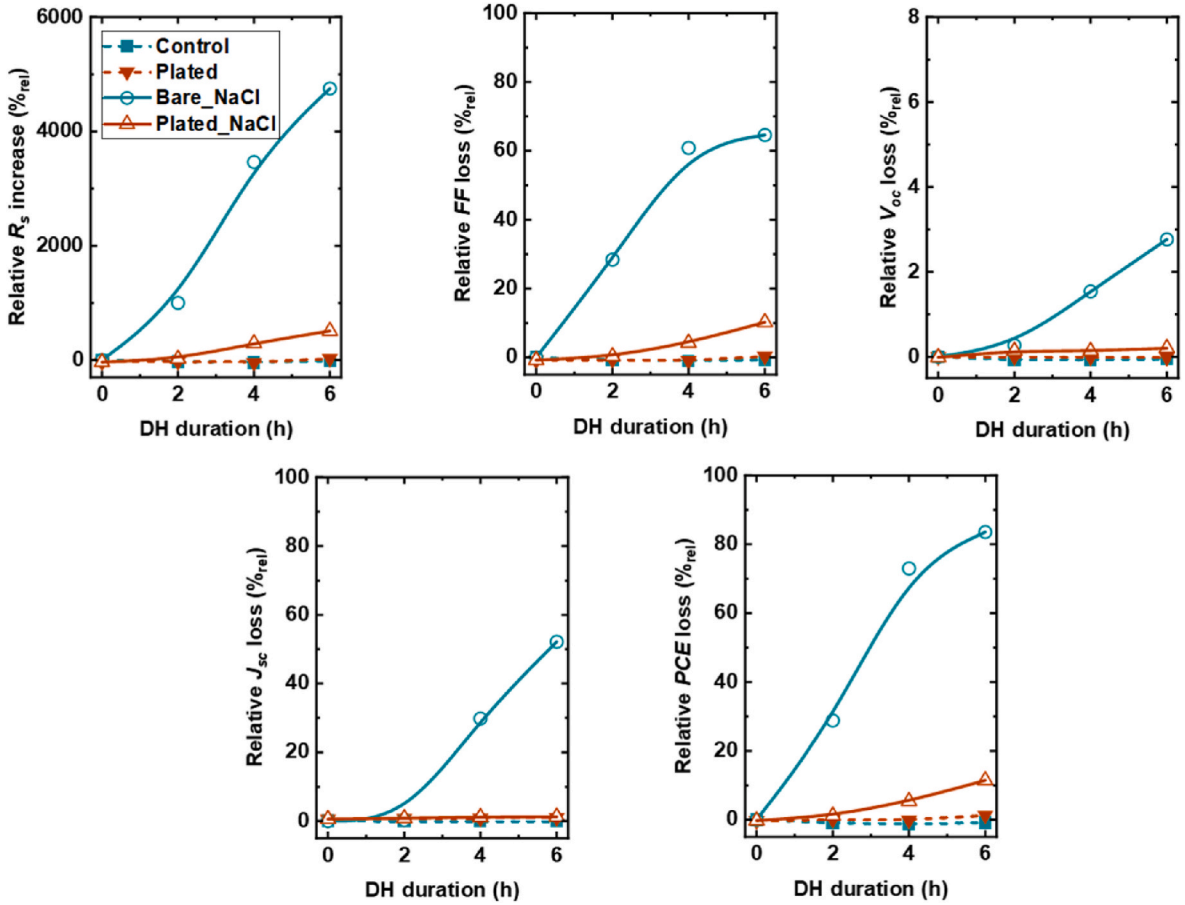

Fig. 6. Relative variations of R_s, FF, V_{oc}, J_{sc} and PCE of all cells shown in Fig. 1 (b) during DH testing.

3.2.2. Series resistance and photoluminescence images

Figs. 7 and 8, respectively, show the R_s and PL images of representative samples of Group Control, Plated, Bare_NaCl and Plated_NaCl, which were captured at designated intervals by removing the solar cells from the climate chamber during the DH experiments. For the Control and Plated samples, no noteworthy degradation could be observed from either R_s or PL images, which is in good agreement with the I-V results in Fig. 6. However, notable R_s issues can be observed for the Bare_NaCl sample after only 2 h of DH testing, which deteriorated further after 4 and 6 h of DH testing. Meanwhile, the Plated_NaCl sample also showed a slight R_s issue with fabric-like patterns in the R_s image after the DH testing, but compared with the Bare_NaCl sample, the Plated_NaCl sample was a lot more stable.

On the other hand, no significant changes were revealed in the PL images of both Bare_NaCl and Plated_NaCl samples, indicating that the DH testing did not significantly increase the recombination all over the TOPCon solar cells in this study. However, the locally magnified images revealed that the Bare_NaCl sample exhibited a blurry signal along the metal contact region, suggesting that the front passivation layer is stable under the DH condition, and NaCl-induced recombination primarily occurred at the contact after the DH testing. In contrast, the PL image of the Plated_NaCl sample was notably brighter around the contacted region, in good agreement with the more stable V_{oc} performance derived from the I-V measurement. The results could also explain why the plated-Cu, which just covered the metal instead of the whole area of the cells, was able to protect cells from NaCl-induced degradation.

3.2.3. Four-point probe and TLM measurement results

Based on both I-V and luminescence results, the major problem of the samples that showed a decrease in performance was the rapid increase of R_s. Therefore, four-point probe and TLM measurements were carried out to study the resistive losses in more detail. Fig. 9 (a) presents the line resistance of samples after 6 h of DH testing, measured on fingers without the presence of busbars, by a four-point probe station. The line resistances of Bare_NaCl and Plated_NaCl samples were obtained for comparison, and samples from the Control and Plated Group were also measured as references to exclude the effect of the additional plated-Cu layer itself on the line resistance measurement. According to the results, the Plated samples had lower line resistance than the Control samples, mainly due to the larger cross-section area with the presence of the plated-Cu layer. Surprisingly, both the Bare_NaCl and Plated_NaCl samples showed slightly higher line resistance than the Control and Plated samples, respectively, indicating a quite minor NaCl-induced degradation in the metal bulk. The effect of the higher line resistances on the FF was then calculated by Griddler 2.5 PRO [58] simulations. The simulation results indicated that the increase of line resistance only leads to ~1.56%$_{rel}$ higher R_s for the bare samples and ~0.88%$_{rel}$ for the plated samples, respectively. This indicates that the increase in R_s for both the bare and plated samples cannot be attributed to an increase in line resistance.

On the contrary, a severe increase was observed in the contact resistivity of samples. Fig. 9 (b) shows the measured contact resistivity results of NaCl-exposed samples during DH testing. It clearly shows that without the protection layer, the contact resistivity of samples increased rapidly during DH testing, which could likely explain the swift R_s increase. Notably, even after 0.5 h of DH testing, a 10-fold increase in contact resistivity is observed. For longer DH testing times, the contact resistance increases for both the bare and plated samples. Notably, the increased contact resistivity of the plated sample could be due to the corrosion of the metal-Si contact and deteriorated Cu. However, it still

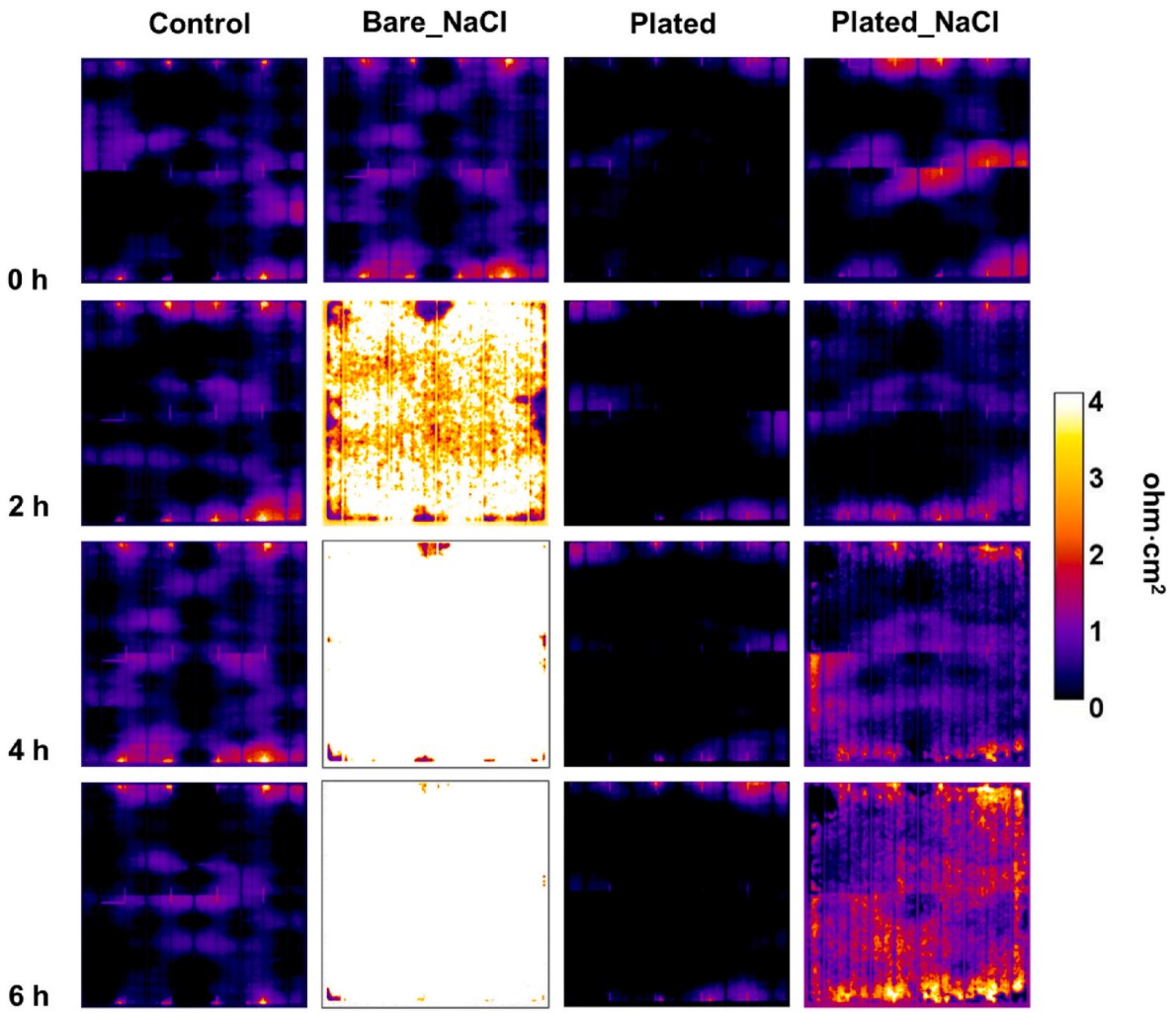

Fig. 7. R_s images of as-received and plated cells exposed to NaCl solution before and after 2, 4 and 6 h of DH testing.

maintains a contact resistance that is at least one order of magnitude lower than its bare counterpart. From this result, it is clear that NaCl severely degraded the metal-Si contact interface without protection and Cu-plating on top of the screen-printed contact is an effective way to protect this interface.

3.2.4. SEM and EDS analysis

The effectiveness of plated-Cu in protecting cells against degradation can be further demonstrated through SEM images, as shown in Fig. 10. Top-view SEM images on the front metal of samples of Group Bare_NaCl and Plated_NaCl were taken to check the morphology after 6 h of DH testing. As shown in Fig. 2 (a), the screen-printed metal contact originally had a porous structure. This porous structure allows for contaminants to enter the contact and react with constituents of the screen-printed contact. The hypothesis is supported by Fig. 10 (a), presenting the front metal of the Bare_NaCl sample after 6 h of DH testing. A high concentration of needle-like particles is visible at the ravine of the porous surface, indicating pronounced corrosion during DH testing [19]. In contrast, the surface of plated contact was much more compact. Fig. 10 (b) shows that after 6 h of DH testing, the contact morphology of the plated-Cu became squaliform, illustrating slight Cu corrosion. This contrasts with the smoother surface before DH testing in Fig. 2 (b). However, the metal contacts remained significantly denser compared to those without copper plating. As a result, despite slight degradation that appeared on the surface of the plated-Cu, the plated-Cu could still play a protective role on the top of the printed metal. Thus, performance degradation was slower compared to samples without plated-Cu. Consequently, it could be deduced from the surface morphology that applying Cu plating can reduce the porosity of the metal surface, slowing down ion penetration and mitigating TOPCon front contact degradation.

Moreover, based on the results discussed in previous sections, the degradation caused by NaCl solution during DH testing was mainly attributed to the corrosion taking place at the interface between Si and metal. To have a deeper understanding of the degradation and the protective effect, a detailed analysis was conducted by using Cryo-FIB to capture cross-sectional SEM and EDS results. In Fig. 11, the front metal of Bare_NaCl, and Plated_NaCl samples after 6 h of DH testing were presented for comparison. The element signals of Ag, Na, and Cl for both samples and also Cu signal for samples with plated-Cu (Plated_NaCl group) are also shown.

As shown in Fig. 11 (a), pronounced Na and Cl signals could be observed in the contaminated samples without Cu (Bare_NaCl). The results clearly show that both Na and Cl were not only detected in the finger bulk but also close to the metal-Si interface. Moreover, the positions of Na and Cl signals are not consistent, indicating those two elements did not move into the metal bulk together as a compound. Therefore, under the DH conditions, the high-mobility Na^+ and Cl^- might swiftly penetrate from the metal surface to the metal bulk and even metal-Si contact through the observed pores and voids. The separate presence of Na^+ and Cl^- also indicates an electrochemical reaction with the metal-Si contact. As reported, the ions could react with components (Ag, glass frit, etc.) of the TOPCon cell front metal paste and

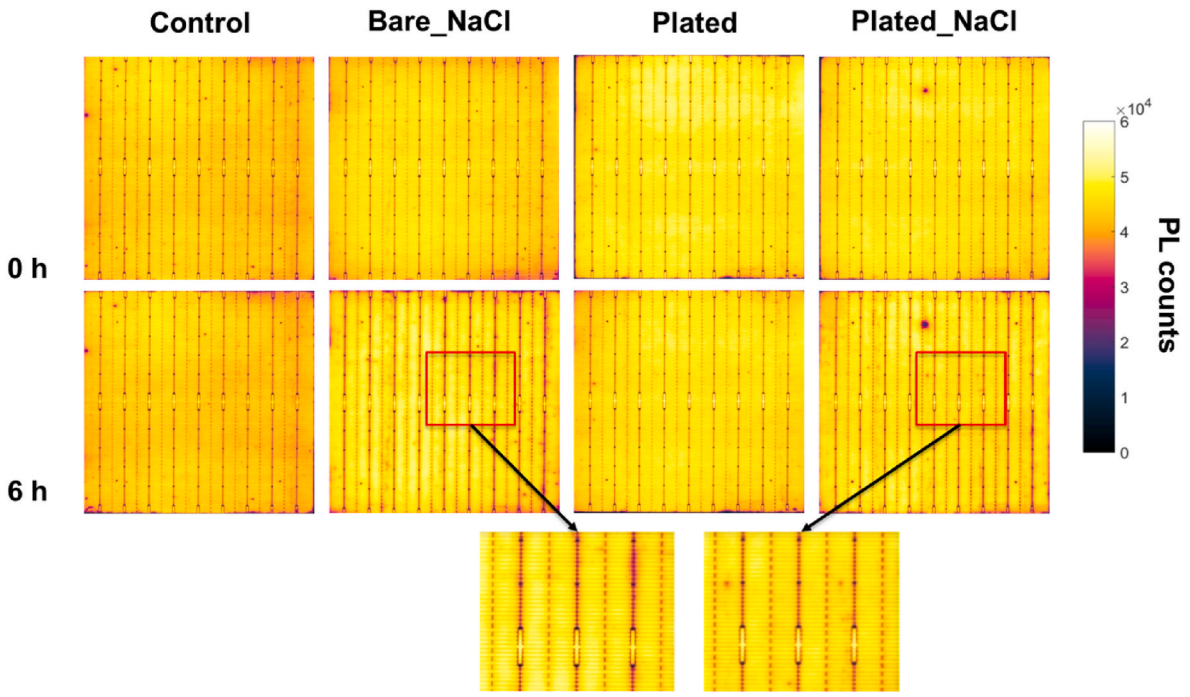

Fig. 8. PL images of as-received and plated cells exposed to NaCl before and after 6 h of DH testing.

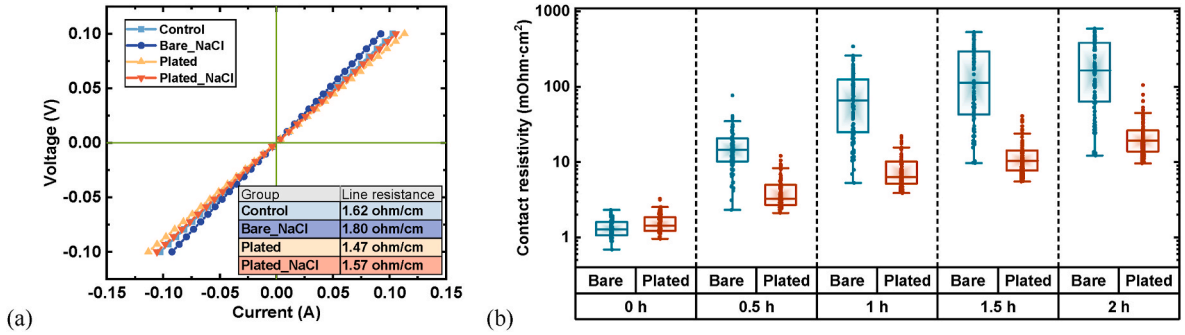

Fig. 9. (a) Line resistance of bare and plated cells with pre-exposure to NaCl solution after 6 h of DH testing, and the line resistance of control and plated samples without contamination were also measured for comparison. (b) Contact resistivity as a function of DH time of samples with or without plated-Cu. All samples were pre-exposed to NaCl.

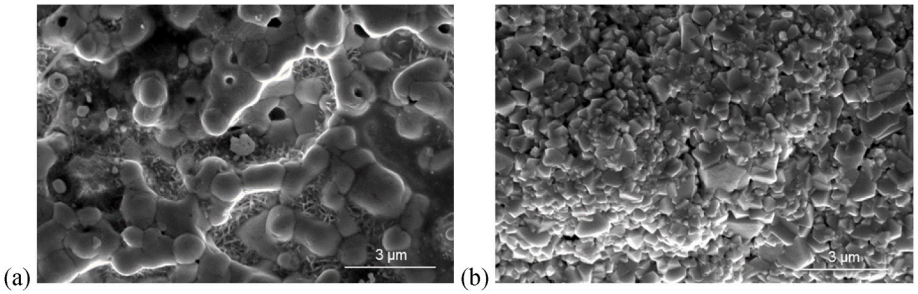

Fig. 10. Top-view SEM images of the front metal contact of (a) Group Bare_NaCl and (b) Group Plated_NaCl after DH testing.

thus lead to severe corrosion [25] and electrical degradation. Additionally, our previous work [26] also demonstrated that the aluminum (Al) additive of the TOPCon front metal paste was sensitive to corrosion by NaCl during the DH testing. With the presence of relatively high temperature and humidity, the oxidation of Al caused by corrosive ions (Cl^- in our case) could be further accelerated. Notably, deterioration of the metal-Si contact, as marked in the SEM image of the Bare_NaCl sample, highly overlapped with the signal of Cl. Considering the conditions of glass frit and additives of the paste were important to keep the adhesive strength of the metal-Si interface and ensure a good quality ohmic contact, the presence of corrosive ions at the interface should be responsible for the severe degradation of the contact components and lead to rapid increase of contact resistance, shown in Fig. 9 (b). Interestingly, according to I-V results, the plated-Cu significantly alleviated

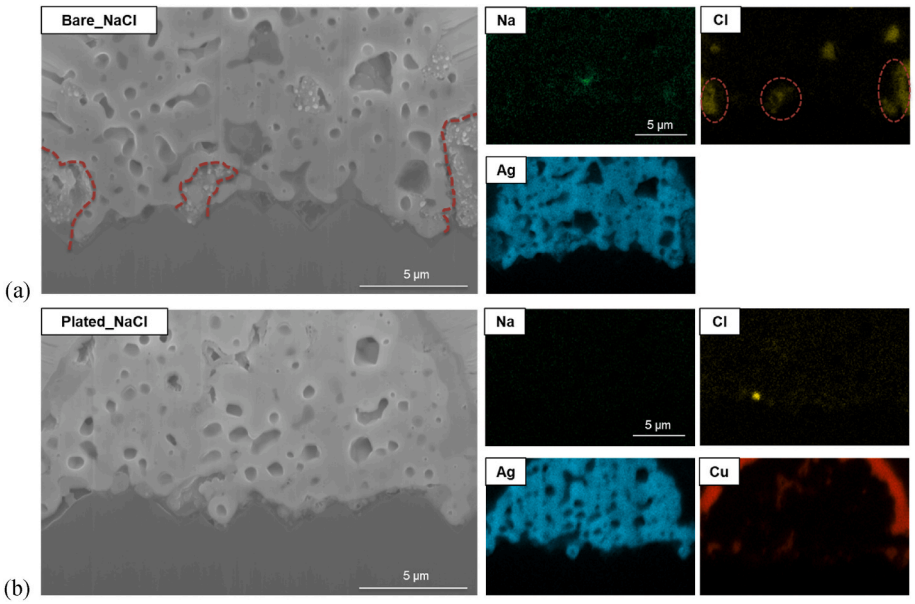

Fig. 11. Cross-sectional SEM images of (a) Bare_NaCl, and (b) Plated_NaCl samples after DH testing and corresponding EDS mappings, including Ag, Na, and Cl for all samples, and also Cu for plated samples.

the NaCl-induced degradation and slowed down the increase of R_s. Fig. 11 (b) shows the SEM and EDS of the plated sample with exposure to NaCl solution (Plated_NaCl). Only a small Cl signal can be observed near the contact, and almost no Na signal could be detected after 6 h of DH testing. This results in significantly reduced contact corrosion compared to bare samples, leading to only a slight *PCE* degradation, as illustrated in Fig. 6.

Moreover, a detailed EDS analysis was conducted to quantify the amount of contaminants in both samples. As EDS is a localized characterization analysis, the fractions of natural components (Ag, Si, Al, Pb, etc.) of the metal contact slightly varied with the location of the FIB cutting. Therefore, it might not be appropriate to directly compare the absolute atomic fractions of contaminants between two samples. Instead, to make the analysis more convincing, the atomic fraction of Ag was chosen as a reference, and the atomic ratios of Na and Cl to Ag of the two samples were compared and shown in Table 3, which could also prove the protective effect of the plated-Cu. Notably, both two elements showed significant differences between samples with or without Cu protection. Regarding the Bare_NaCl sample, the atomic ratio of Na to Ag achieved around 1.36 % in the cross-sectional area. However, no significant Na signal could be detected in Plated-NaCl samples. Both are consistent with EDS mapping results. Additionally, the ratio of Cl to Ag also decreased greatly with the presence of plated-Cu. As expected, the Cl/Ag of the Plated_NaCl sample was found to be ~0.22 %, which is much lower than that of Bare_NaCl (~2.33 %), agreeing with the EDS mapping again. The results further confirmed our hypothesis that the dense plated-Cu layer can mitigate the penetration of ions through the surface of metal due to the natural porous structure. The EDS mapping and atomic fractions of Na and Cl provided insights into a reduced R_s increase and V_{oc} decrease. Therefore, the results revealed the protection mechanism of plated-Cu. The plated-Cu acts as a barrier layer by covering the metal surface and filling voids. In that way, the in-diffusion of contaminants was significantly alleviated. Consequently, the plated-Cu effectively protects the solar cells from severe contact corrosion and performance degradation.

Table 3
The EDS elemental atomic ratio of Na and Cl to Ag for the Bare_NaCl and Plated_NaCl samples shown in the cross-sectional SEM images in Fig. 11.

Atomic ratio (%)	Na/Ag	Cl/Ag
Bare_NaCl	1.36	2.33
Plated_NaCl	0.00	0.22

4. Conclusion

TOPCon cells with Al-containing front Ag-paste are reported to be quite sensitive to the contaminants under 85 °C and 85 % relative humidity accelerated damp-heat (DH) test. The study utilized bias-assisted light-induced plating to grow ~1 μm Cu on the front grid of TOPCon cells to improve its stability. The as-plated cell efficiency was ~0.09%$_{abs}$ higher than the as-received TOPCon solar cell due to an increased fill factor. NaCl was chosen as a representative contaminant to conduct an accelerated cell-level damp heat test. The I-V results showed a rapid R_s increase and V_{oc} drop, resulting in over 80%$_{rel}$ efficiency degradation for the non-plated TOPCon solar cells after 6 h of DH testing. However, the Cu-plated samples performed much better under the same conditions with only a ~11.5%$_{rel}$ drop in *PCE* after 6 h of DH testing, resulting from a slight R_s increase. Considering the results of this accelerated test, we conclude the plated-Cu layer can effectively alleviate NaCl-induced degradation under DH conditions and highly improve the device stability. The electrical performance of cells was also confirmed by PL and R_s images. Additionally, the contact resistivity of NaCl-exposed bare cells was already 1 to 2 orders of magnitude higher than that of plated cells after just 2 h of DH testing, explaining most of the loss in *FF*. The following detailed SEM and EDS analysis showed that the degradation mainly took place at the metal contact region. It illustrated that during DH testing, ions might diffuse through the holes of metal and trigger potential electrochemical reactions with the Ag, glass frit, and additives of the TOPCon cell front metal paste. The reactions then lead to higher contact resistance and also parasitic recombination at the contact region. Fortunately, the plated-Cu is dense enough to cover the metal surface and fill the voids to make the whole contact more compact. Therefore, the penetration of ions is hindered and contact is more stable during DH testing. The results showed the potential of reducing Ag consumption and cost with better electrical performance as well as higher resistance to contaminant-induced degradation during the operation in the field. Consequently, our work offers a pathway to photovoltaic technology with a longer lifetime and lower LCOE.

CRediT authorship contribution statement

Xutao Wang: Writing – original draft, Visualization, Methodology, Investigation, Formal analysis, Data curation, Conceptualization. **Chandany Sen:** Writing – review & editing, Supervision, Methodology, Investigation, Formal analysis, Data curation. **Xinyuan Wu:** Methodology, Investigation, Formal analysis. **Yuan-Chih Chang:** Methodology, Investigation. **Haoran Wang:** Investigation, Formal analysis. **Muhammad Umair Khan:** Writing – review & editing, Investigation. **Bram Hoex:** Writing – review & editing, Visualization, Supervision, Project administration, Funding acquisition, Formal analysis, Conceptualization.

Declaration of competing interest

The authors declare the following financial interests/personal relationships which may be considered as potential competing interests: Bram Hoex reports financial support was provided by Australian Renewable Energy Agency. Bram Hoex reports financial support was provided by Australian Centre for Advanced Photovoltaics. Bram Hoex reports financial support was provided by Trailblazer for Recycling & Clean Energy program. Bram Hoex, Chandany Sen, Xinyuan Wu, Yuan-Chih Chang and Xutao Wang have patent #Australian application number 2024903846 issued to University of New South Wales. If there are other authors, they declare that they have no known competing financial interests or personal relationships that could have appeared to influence the work reported in this paper.

Acknowledgments

This research work was supported by the Australian Government through the Australian Renewable Energy Agency (ARENA 1–060 Extension project) and the Australian Centre for Advanced Photovoltaics (ACAP), also funded by ARENA. The authors appreciate support provided by the Australian Government's Trailblazer for Recycling & Clean Energy program, led by UNSW & the University of Newcastle. The Australian Government bears no responsibility for the views, information, or advice expressed in this research. The authors gratefully acknowledge the assistance from Dr. Yin Yao and Dr. Charlie Kong, and access to the scanning electron microscopy (SEM450) and ZEISS Cryogenic focused ion beam (Cryo-FIB) tool provided by the Electron Microscope Unit at The University of New South Wales (UNSW). Additionally, the authors extend their gratitude for the help from Dr. Zhenyu Sun and Yuhao Cheng with the four-point probe station measurement and also for the support received from the UNSW Tyree Energy Technologies Building (TETB) and Solar Industrial Research Facility (SIRF) LDOT team. Xutao Wang acknowledges the University International Postgraduate Award (UIPA) Scholarship support from UNSW.

Data availability

Data will be made available on request.

References

[1] ITRPV, International Technology Roadmap for Photovoltaic, 2024.
[2] H. Ullah, S. Czapp, S. Szultka, H. Tariq, U.B. Qasim, H. Imran, Crystalline silicon (c-Si)-Based tunnel oxide passivated contact (TOPCon) solar cells: a review, Energies 16 (2023) 715, https://doi.org/10.3390/en16020715.
[3] F. Feldmann, C. Reichel, R. Müller, M. Hermle, The application of poly-Si/SiOx contacts as passivated top/rear contacts in Si solar cells, Sol. Energy Mater. Sol. Cell. 159 (2017) 265–271, https://doi.org/10.1016/j.solmat.2016.09.015.
[4] D.K. Ghosh, S. Bose, G. Das, S. Acharyya, A. Nandi, S. Mukhopadhyay, A. Sengupta, Fundamentals, present status and future perspective of TOPCon solar cells: a comprehensive review, Surface. Interfac. 30 (2022) 101917, https://doi.org/10.1016/j.surfin.2022.101917.
[5] B. Liao, W. Wu, R.J. Yeo, X. Wu, S. Ma, Q. Wang, Y. Wan, X. Su, W. Shen, X. Li, W. Li, G. Xing, B. Hoex, Atomic scale controlled tunnel oxide enabled by a novel industrial tube-based PEALD technology with demonstrated commercial TOPCon cell efficiencies > 24, Prog. Photovoltaics Res. Appl. 31 (2023) 220–229, https://doi.org/10.1002/pip.3627.
[6] V. Kanneboina, Detailed review on c-Si/a-Si:H heterojunction solar cells in perspective of experimental and simulation, Microelectron. Eng. 265 (2022) 111884, https://doi.org/10.1016/j.mee.2022.111884.
[7] M. Sharma, J. Panigrahi, V.K. Komarala, Nanocrystalline silicon thin film growth and application for silicon heterojunction solar cells: a short review, Nanoscale Adv. 3 (2021) 3373–3383, https://doi.org/10.1039/d0na00791a.
[8] O. Arriaga Arruti, A. Virtuani, C. Ballif, Long-term performance and reliability of silicon heterojunction solar modules, Prog. Photovoltaics Res. Appl. 31 (2023) 664–677, https://doi.org/10.1002/pip.3688.
[9] A. Razzaq, T.G. Allen, W. Liu, Z. Liu, S. De Wolf, Silicon heterojunction solar cells: techno-economic assessment and opportunities, Joule 6 (2022) 514–542, https://doi.org/10.1016/j.joule.2022.02.009.
[10] EU/Trinasolar announces efficiency of 26.58% for its n-type TOPCon cells, setting a new world record, Trina Solar. https://static.trinasolar.com/eu-en/resources/newsroom/eu-trinasolar-announces-efficiency-2658-its-n-type-topcon-cells-setting-new-world, 2024 (accessed December 9, 2024).
[11] Trina Solar claims record-breaking efficiency of 26.58% for TOPCon solar cell, Pv Magazine International (2024). https://www.pv-magazine.com/2024/11/21/trina-solar-claims-record-breaking-efficiency-of-26-58-for-topcon-solar-cell/ (accessed December 9, 2024).
[12] M. Woodhouse, D. Feldman, R. Fu, K. Horowitz, D. Chung, On the path to SunShot: the role of advancements in solar photovoltaic efficiency, Reliability, and Costs, (n. d.).
[13] I.M. Peters, C.D. Rodriguez Gallegos, S.E. Sofia, T. Buonassisi, The value of efficiency in photovoltaics, Joule 3 (2019) 2732–2747, https://doi.org/10.1016/j.joule.2019.07.028.
[14] I.M. Peters, J. Hauch, C. Brabec, P. Sinha, The value of stability in photovoltaics, Joule 5 (2021) 3137–3153, https://doi.org/10.1016/j.joule.2021.10.019.
[15] A. Richter, M. Hermle, S.W. Glunz, Reassessment of the limiting efficiency for crystalline silicon solar cells, IEEE J. Photovoltaics 3 (2013) 1184–1191, https://doi.org/10.1109/JPHOTOV.2013.2270351.
[16] Terrestrial photovoltaic (PV) modules – design qualification and type approval – Part 2: test procedures - edition 2.0 - Engineering Workbench. https://ewb.ihs.com/#/document/LXLESGAAAAAAAAAA?sr=dv-dl&fdocid=VMIESGAAAAAAAAAA&fdocpagenum=11#h017a8be5, 2021. (Accessed 15 March 2024).
[17] W. Oh, S. Kim, S. Bae, N. Park, Y. Kang, H.-S. Lee, D. Kim, The degradation of multi-crystalline silicon solar cells after damp heat tests, Microelectron. Reliab. 54 (2014) 2176–2179, https://doi.org/10.1016/j.microrel.2014.07.071.
[18] F. ibne Mahmood, A. Kumar, M. Afridi, G. TamizhMani, Potential induced degradation in c-Si glass-glass modules after extended damp heat stress, Sol. Energy 254 (2023) 102–111, https://doi.org/10.1016/j.solener.2023.03.013.
[19] C. Peike, S. Hoffmann, P. Hülsmann, B. Thaidigsmann, K.A. Weiβ, M. Koehl, P. Bentz, Origin of damp-heat induced cell degradation, Sol. Energy Mater. Sol. Cell. 116 (2013) 49–54, https://doi.org/10.1016/j.solmat.2013.03.022.
[20] K. Hara, Raman spectroscopic analysis of encapsulants in aged photovoltaic modules, J. Photochem. Photobiol. Chem. 425 (2022) 113721, https://doi.org/10.1016/j.jphotochem.2021.113721.
[21] C. Sen, H. Wang, X. Wu, M.U. Khan, C. Chan, M. Abbott, B. Hoex, Four failure modes in silicon heterojunction glass-backsheet modules, Sol. Energy Mater. Sol. Cell. 257 (2023) 112358, https://doi.org/10.1016/j.solmat.2023.112358.
[22] N. Iqbal, M. Li, T.S. Sakthivel, K. Mikeska, M. Lu, N. Nandakumar, S. Duttagupta, M. Dhamrin, K. Tsuji, S. Bowden, A. Augusto, Y. Guan, S. Seal, K.O. Davis, Impact of acetic acid exposure on metal contact degradation of different crystalline silicon solar cell technologies, Sol. Energy Mater. Sol. Cell. 250 (2023) 112089, https://doi.org/10.1016/j.solmat.2022.112089.
[23] P.M. Sommeling, J. Liu, J.M. Kroon, Corrosion effects in bifacial crystalline silicon PV modules; interactions between metallization and encapsulation, Sol. Energy Mater. Sol. Cell. 256 (2023) 112321, https://doi.org/10.1016/j.solmat.2023.112321.
[24] Y. Zhou, D. Chen, Y. Ye, H. Yin, X. Niu, Damp-heat endurance investigation of PV modules based on n-type bifacial passivated contact cells, in: 40th European Photovoltaic Solar Energy Conference and Exhibition, 2023.
[25] C. Sen, X. Wu, H. Wang, M.U. Khan, L. Mao, F. Jiang, T. Xu, G. Zhang, C. Chan, B. Hoex, Accelerated damp-heat testing at the cell-level of bifacial silicon HJT, PERC and TOPCon solar cells using sodium chloride, Sol. Energy Mater. Sol. Cell. 262 (2023) 112554, https://doi.org/10.1016/j.solmat.2023.112554.
[26] X. Wu, X. Wang, W. Yang, J. Nie, J. Yuan, M.U. Khan, A. Ciesla, C. Sen, Z. Qiao, B. Hoex, Enhancing the reliability of TOPCon technology by laser-enhanced contact firing, Sol. Energy Mater. Sol. Cell. 271 (2024) 112846, https://doi.org/10.1016/j.solmat.2024.112846.
[27] C. Sen, H. Wang, M.U. Khan, J. Fu, X. Wu, X. Wang, B. Hoex, Buyer aware: three new failure modes in TOPCon modules absent from PERC technology, Sol. Energy Mater. Sol. Cell. 272 (2024) 112877, https://doi.org/10.1016/j.solmat.2024.112877.
[28] X. Wu, C. Sen, X. Wang, Y. Cheng, R. Lv, H. Song, Y. Yu, B. Liao, S. Ma, M.U. Khan, A. Ciesla, B. Hoex, Unveiling the origin of metal contact failures in TOPCon solar cells through accelerated damp-heat testing, Sol. Energy Mater. Sol. Cell. 278 (2024) 113188, https://doi.org/10.1016/j.solmat.2024.113188.
[29] D. Kapila, J.L. Plawsky, Diffusion processes for integrated waveguide fabrication in glasses: a solid-state electrochemical approach, Chem. Eng. Sci. 50 (1995) 2589–2600, https://doi.org/10.1016/0009-2509(95)00115-L.
[30] Q. Bai, H. Yang, C. Nan, H. Wang, Z. Chen, Analysis of the electrochemical reactions and ions migration for crystalline silicon solar module under high system

voltage, Sol. Energy 225 (2021) 718–725, https://doi.org/10.1016/j.solener.2021.07.050.
[31] M.U. Khan, C. Sen, C. Chan, M. Abbott, G. Poduval, Y. Wu, R. Lv, G. Zhang, B. Hoex, Supercharging cell-level potential-induced degradation (PID) testing using a salt-enriched hybrid polymer layer, Sol. Energy Mater. Sol. Cell. 260 (2023) 112479, https://doi.org/10.1016/j.solmat.2023.112479.
[32] D. Adachi, T. Terashita, T. Uto, J.L. Hernández, K. Yamamoto, Effects of SiOx barrier layer prepared by plasma-enhanced chemical vapor deposition on improvement of long-term reliability and production cost for Cu-plated amorphous Si/crystalline Si heterojunction solar cells, Sol. Energy Mater. Sol. Cell. 163 (2017) 204–209, https://doi.org/10.1016/j.solmat.2016.12.029.
[33] X. Wu, C. Sen, H. Wang, X. Wang, Y. Wu, M.U. Khan, L. Mao, F. Jiang, T. Xu, G. Zhang, B. Hoex, Addressing sodium ion-related degradation in SHJ cells by the application of nano-scale barrier layers, Sol. Energy Mater. Sol. Cell. 264 (2024) 112604, https://doi.org/10.1016/j.solmat.2023.112604.
[34] L. Pirot-Berson, R. Couderc, R. Bodeux, J. Dupuis, Failure modes of silicon heterojunction photovoltaic modules in damp heat environment: sodium and moisture effects, Sol. Energy Mater. Sol. Cell. 278 (2024) 113190, https://doi.org/10.1016/j.solmat.2024.113190.
[35] X. Wu, X. Wang, R. Lv, H. Song, Y. Yu, C. Sen, Y. Cheng, M.U. Khan, A. Ciesla, T. Xu, G. Zhang, B. Hoex, Unveiling the degradation mechanisms in silicon heterojunction solar cells under accelerated damp-heat testing, Sol. Energy Mater. Sol. Cell. 282 (2025) 113325, https://doi.org/10.1016/j.solmat.2024.113325.
[36] A. Majumdar, D. Samanta, R. Das, Chemical characteristics and trends of Indian summer monsoon rainfall: a review, Aerosol Air Qual. Res. 22 (2022) 220019, https://doi.org/10.4209/aaqr.220019.
[37] S. Norela, M.S. Saidah, M. Mahmud, Chemical composition of the haze in Malaysia 2005, Atmos. Environ. 77 (2013) 1005–1010, https://doi.org/10.1016/j.atmosenv.2013.05.024.
[38] J.L. Bischoff, R.J. Rosenbauer, An empirical equation of state for hydrothermal seawater (3.2 percent NaCl), Am. J. Sci. 285 (1985) 725–763, https://doi.org/10.2475/ajs.285.8.725.
[39] O.K. Segbefia, N. Akhtar, T.O. Sætre, Moisture induced degradation in field-aged multicrystalline silicon photovoltaic modules, Sol. Energy Mater. Sol. Cell. 258 (2023) 112407, https://doi.org/10.1016/j.solmat.2023.112407.
[40] N.G. Dhere, N.R. Raravikar, Adhesional shear strength and surface analysis of a PV module deployed in harsh coastal climate, Sol. Energy Mater. Sol. Cell. 67 (2001) 363–367, https://doi.org/10.1016/S0927-0248(00)00304-4.
[41] Photovoltaic (PV) modules – salt mist corrosion testing - edition 3.0 - engineering workbench. https://ewb.ihs.com/#/document/YWQXMGAAAAAAAAAA?qid=63869309714569456&sr=re-1-10&kbid=4%7C20027&docid=944225210#ha48be5fc, 2020 (accessed December 9, 2024).
[42] X. Li, Y. Yang, K. Jiang, S. Huang, W. Zhao, Z. Li, G. Wang, A. Han, J. Yu, D. Li, F. Meng, L. Zhang, Z. Liu, W. Liu, Potential-free sodium-induced degradation of silicon heterojunction solar cells, Prog. Photovoltaics Res. Appl. 31 (2023) 939–948, https://doi.org/10.1002/pip.3698.
[43] L. Zhao LibinMo, C. Zhou, G. Wang, X. Jia, W. Wang, Ag/Cu plating to improve Ag grid electrodes of the recycled c-Si solar cells, Int. J. Electrochem. Sci. 15 (2020) 11920–11928, https://doi.org/10.20964/2020.12.77.
[44] S.H. Lee, D.W. Lee, A. ur Rehman, J.W. Baik, S.H. Lee, Study of annealing temperature for Ni/Cu/Ag plated front contact single crystalline solar cells, IEEE J. Photovoltaics 6 (2016) 1090–1093, https://doi.org/10.1109/JPHOTOV.2016.2576683.
[45] A. Büchler, S. Kluska, J. Bartsch, G. Cimiotti, A.A. Brand, M.C. Schubert, M. Glatthaar, Optimizing adhesion of laser structured plated Ni-Cu contacts with insights from micro characterization, Energy Proc. 92 (2016) 913–918, https://doi.org/10.1016/j.egypro.2016.07.101.
[46] S. Kluska, B. Grübel, G. Cimiotti, C. Schmiga, H. Berg, A. Beinert, I. Kubitza, P. Müller, T. Voss, Plated TOPCon solar cells & modules with reliable fracture stress and soldered module interconnection, EPJ Photovolt 12 (2021) 10, https://doi.org/10.1051/epjpv/2021010.
[47] M. Aleem, R. Vishnuraj, B. Krishnan, B. Pullithadathil, Realization of micropatterned, narrow line-width Ni–Cu–Sn front contact grid pattern using maskless direct-write lithography for industrial silicon solar cells, ACS Appl. Energy Mater. 4 (2021) 10682–10696, https://doi.org/10.1021/acsaem.1c01699.
[48] Y. Zeng, C.-W. Peng, W. Hong, S. Wang, C. Yu, S. Zou, X. Su, Review on metallization approaches for high-efficiency silicon heterojunction solar cells, Trans. Tianjin Univ. 28 (2022) 358–373, https://doi.org/10.1007/s12209-022-00336-9.
[49] D.N.R. Payne, C. Vargas, Z. Hameiri, S.R. Wenham, D.M. Bagnall, An advanced software suite for the processing and analysis of silicon luminescence images, Comput. Phys. Commun. 215 (2017) 223–234, https://doi.org/10.1016/j.cpc.2017.02.012.
[50] C.A. Schneider, W.S. Rasband, K.W. Eliceiri, NIH Image to ImageJ: 25 years of image analysis, Nat. Methods 9 (2012) 671–675, https://doi.org/10.1038/nmeth.2089.
[51] A. Lennon, J. Colwell, K.P. Rodbell, Challenges facing copper-plated metallisation for silicon photovoltaics: insights from integrated circuit technology development, Prog. Photovoltaics Res. Appl. 27 (2019) 67–97, https://doi.org/10.1002/pip.3062.
[52] A.A. Istratov, E.R. Weber, Electrical properties and recombination activity of copper, nickel and cobalt in silicon, Appl Phys A 66 (1998) 123–136, https://doi.org/10.1007/s003390050649.
[53] A.A. Istratov, C. Flink, H. Hieslmair, S.A. McHugo, E.R. Weber, Diffusion, solubility and gettering of copper in silicon, Mater. Sci. Eng., B 72 (2000) 99–104, https://doi.org/10.1016/S0921-5107(99)00514-0.
[54] A. Kraft, C. Wolf, J. Bartsch, M. Glatthaar, S. Glunz, Long term stability of copper front side contacts for crystalline silicon solar cells, Sol. Energy Mater. Sol. Cell. 136 (2015) 25–31, https://doi.org/10.1016/j.solmat.2014.12.024.
[55] H. Miyazaki, H. Kojima, K. Hinode, Passivation effect of silicon nitride against copper diffusion, J. Appl. Phys. 81 (1997) 7746–7750, https://doi.org/10.1063/1.365380.
[56] M. Yukawa, H. Kitagawa, S. Iida, Effects of Ag thickness and deposition temperature on prevention of Cu diffusion in Cu/Ag/Si system, Jpn. J. Appl. Phys. 44 (2005) 3187, https://doi.org/10.1143/JJAP.44.3187.
[57] Y.-C. Chang, Y. Zhang, L. Wang, S. Wang, H. Wang, C.-Y. Huang, R. Chen, C. Chan, B. Hallam, Silver-lean metallization and hybrid contacts via plating on screen-printed metal for silicon solar cells manufacturing, Prog. Photovolt.: Res. App. n/a (n.d.). https://doi.org/10.1002/pip.3799.
[58] Griddler_and_PRO_manual.pdf, (n.d.). https://griddlersolar.com/wp-content/uploads/Griddler_and_PRO_manual.pdf (accessed June 5, 2024).